Use of Fischer plots to define third-order sea-level curves in Ordovician peritidal cyclic carbonates, Appalachians

J. F. Read Department of Geological Sciences, Virginia Polytechnic Institute and State University, Blacksburg, Virginia 24061
R. K. Goldhammer* Department of Earth and Planetary Sciences, Johns Hopkins University, Baltimore, Maryland 21218

ABSTRACT

Fischer plots in which cumulative cycle thickness corrected for linear subsidence is plotted against time were originally used in the study of Triassic peritidal sequences to define short-duration departures in relative sea level in the Milankovitch range (10^4 to 10^5 yr). However, they also provide a means of assessing magnitude of third-order (1 to 10 m.y.) fluctuations in sea level which, on the basis of their regional correlatability, we ascribe to eustatic events.

INTRODUCTION

Fischer (1964) introduced the concept that if cumulative cycle thickness of peritidal carbonates were corrected for linear subsidence and plotted against time, using an average cycle period, then the plots highlighted departures in relative sea level (Fig. 1). Fischer (1964) favored pulses of increased subsidence as opposed to eustasy as a cause of these departures. Goldhammer et al. (1987) revived this type of plot to document eustatic fluctuations in sea level within the Milankovitch range of 20 to 100 ka. In addition, Goldhammer (1987) used a Fischer plot of Middle Triassic carbonates in Italy to define third-order sea-level changes.

By using synthetic cyclic carbonate sequences in which the input variables are known, as well as actual examples from Early Ordovician sequences in the Appalachians for which qualitative relative sea-level curves are available (Hardie and Shinn, 1986; Read, 1988a, 1988b), we show that Fischer plots define excursions in relative sea level at the scale of third-order sea-level cycles (1 to 10 m.y.; Vail et al., 1977). The Fischer plot for Pennsylvania (by Goldhammer) was done independently of the plots for Virginia (by Read), thus ruling out observer bias in picking cycle boundaries. They were subsequently replotted using the same time scale. The sea-level curves correlate regionally, indicating that they reflect eustatic sea-level fluctuations. Data from Fischer plots, if corrected for isostatic subsidence and compaction, may provide a quantitative estimate of sea-level fluctuations that can be cross-checked against subsidence modeling techniques of G. C. Bond et al. (in prep.).

FISCHER PLOTS

The concept behind Fischer plots is that any departure from linear subsidence or stable sea level should be evident if cumulative cycle thickness, corrected for linear subsidence, is plotted against time using a calculated average cycle period (Fig. 1).

The Fischer plots are able to define relative sea-level curves because if there is a long-term rise in sea level or an increase in subsidence, relatively thick cycles will develop because accommodation space is increased due to the sea-level rise and water and sediment loading in excess of that due to linear subsidence. The relatively shallow-water character of the peritidal facies, and the low long-term rise rates involved suggest that platform sedimentation rates kept pace with increase in accommodation space. If there is a long-term fall, thin cycles will develop because the falling sea level (or decrease in subsidence rate) decreases the accommodation space expected from linear subsidence. These will be expressed as a positive or negative departure from the horizontal, which defines the level to which the platform would fill through time if sedimentation matched linear subsidence under stable relative sea level; i.e., cycle thicknesses would tend to equal the amount of subsidence per average cycle period.

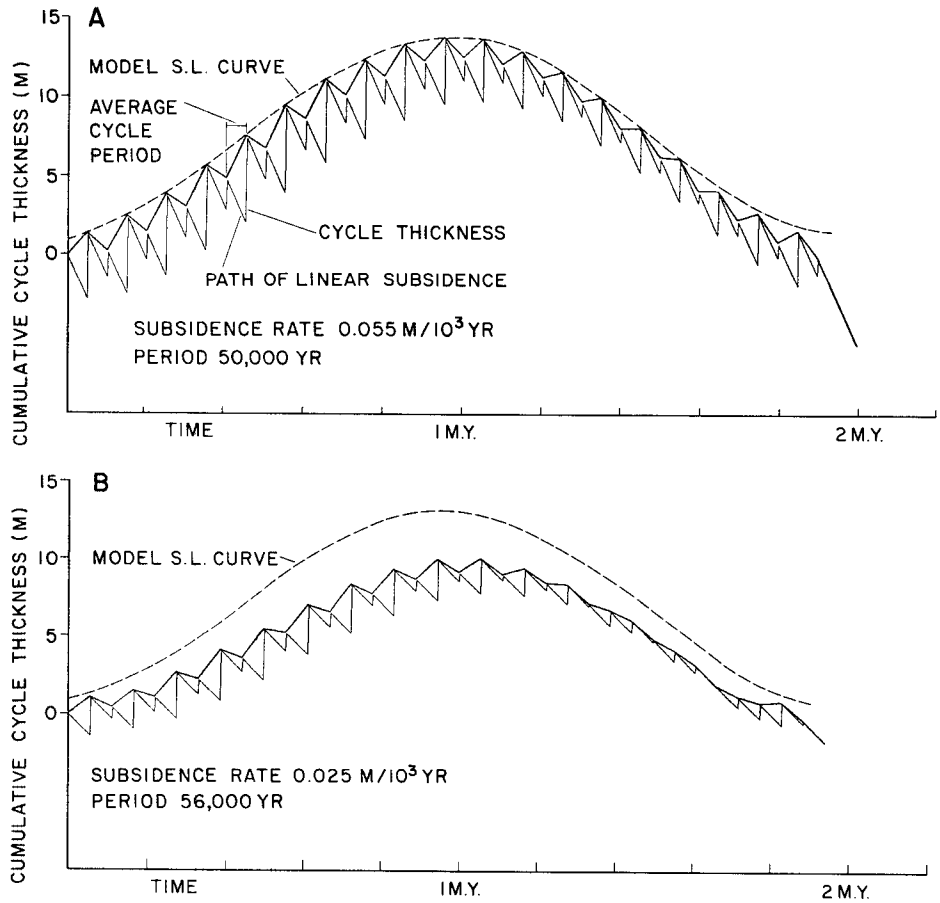

Figure 1. Fischer plots constructed from synthetic carbonate cycles produced by sea-level curve and input variables shown in Figure 2. Fischer diagrams plot cumulative cycle thickness (vertical axis) corrected for linear subsidence (inclined lines sloping to lower right) against time (horizontal axis). Each cycle is assigned average cycle period. Plot is constructed by allowing platform to subside for first cycle period and then plotting thickness of first cycle (vertical line). This is repeated for all cycles; heavy line connecting tops of cycles represents trace of relative sea-level (S.L.) curve. A: Fischer plot of cycles from Figure 2, in which amplitude of third-order sea-level rise was 12.5 m, and subsidence rate was 0.055 m/ka. Dotted line is sea-level curve from model (Fig. 2A). Note coincidence of plot and model curve. B: Fischer plot of cycles from using sea-level curve of Figure 2, but with 0.025 m/ka subsidence rate. Note how this curve does not match model sea-level curve.

*Present address: Exxon Production Research, P.O. Box 2189, Houston, Texas 77001.

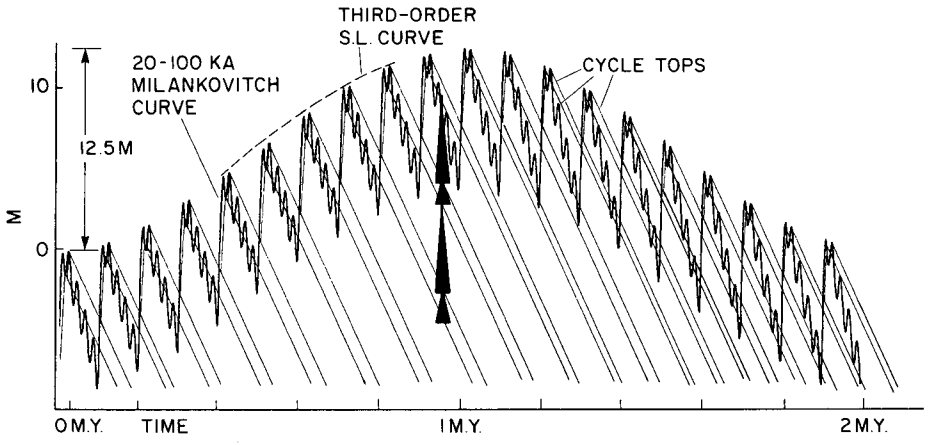

Figure 2. Third-order sea-level curve, amplitude 12.5 m and 2 m.y. duration, with superimposed 100 ka and 20 ka oscillations, which was used to generate cycles in Figure 1. This sea-level curve is used only to illustrate how carbonate cycles and Fischer-plotted, third-order sea-level curves are related; it is not meant to simulate Ordovician cycles. Inclined lines sloping to lower right mark path of subsiding cycle tops. Facies boundaries within cycles not shown. Cycle thickness is measured vertical to horizontal axis of plot, shown by upward-thinning arrows. Enlarged diagrams in Figure 3 show details of synthetic cycles used to construct Fischer plots in Figure 1. Cycle model shows cycles generated by 0.055 m/ka subsidence rate; note that same number of cycles form during third-order rise and fall. With lower subsidence rates, fewer cycles form during third-order fall compared to rise.

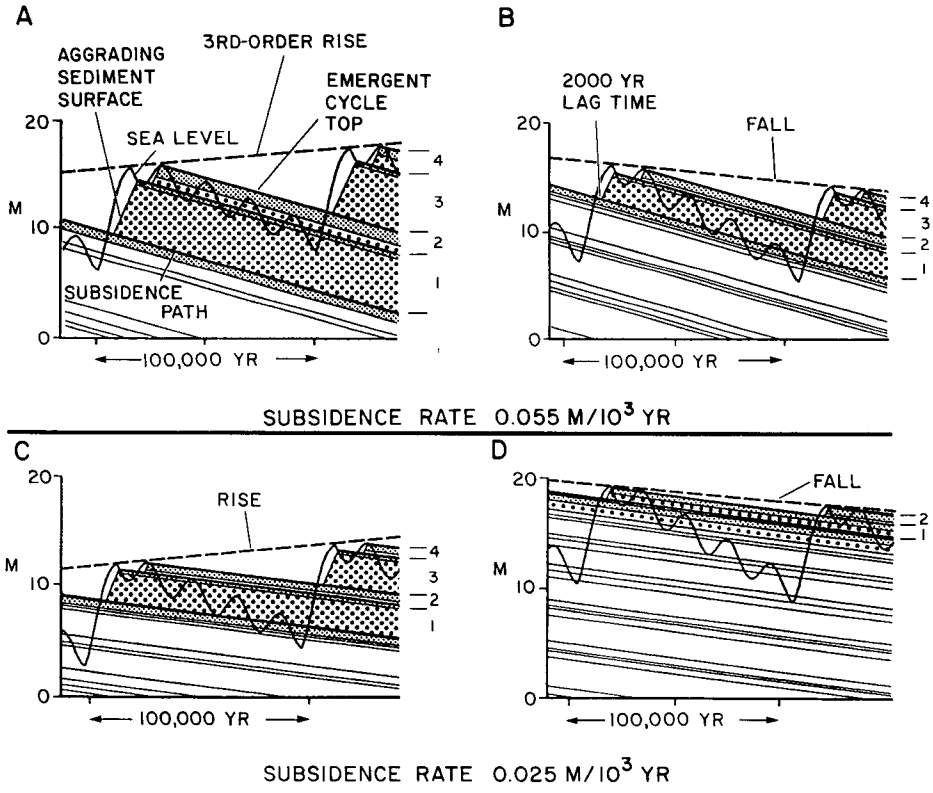

Figure 3. Synthetic cycle models plotted at different scale from that of Figure 2 to illustrate characteristics. Sea-level curve is same as in Figure 2. Lines inclined to lower right mark subsidence paths of facies boundaries and cycle caps; coarse dot pattern = subtidal facies; fine stipple = tidal flat facies. There is 2 ka lag between flooding of platform and sediment upbuilding. Inclined lines sloping to upper right mark path of aggrading sediment surface. A and C show that, for parameters used, similar number of cycles (labeled 1 to 4) form during rise, with 0.055 and 0.025 m/ka subsidence rates, respectively. B and D show cycles formed during long-term fall. Note that in B (0.055 m/ka subsidence), same number of cycles form on third-order fall as on rise, but in D (0.025 m/ka subsidence), fewer cycles form on third-order fall than on rise. This results in Fischer plots showing apparent decreased amplitude of relative sea-level curve for areas of low subsidence rates.

SYNTHETIC CYCLE STRATIGRAPHY

Figures 2 and 3 show how cyclic sequences may be generated with a long-term rise and fall in sea level over 2 m.y.; superimposed are Milankovitch-scale sea-level fluctuations, lag time, sedimentation rate, and linear subsidence (Read et al., 1986). Reasons for using a Milankovitch form to the sea-level curves are outlined in Read (1988b). Note that the form of the high-frequency sea-level curve would not affect the conclusions reached from the modeling, which relate specifically to the low-frequency, long-term sea-level fluctuations. Note that during the long-term rise, the cycles formed tend to be relatively thick (Fig. 3, A and C), whereas those formed during the fall tend to be thin (Fig. 3, B and D). The Fischer plots in Figure 1 were constructed using cycle thicknesses generated by the models illustrated in Figures 2 and 3. Note that the Fischer plots and the synthetic cycle plots have a similar bell shape for the long-term sea-level fluctuation. The Fischer plot in Figure 1A accurately defines the long-term sea-level fluctuation of 12.5 m used in Figure 2. This model involved 0.055 m/ka subsidence rates, and 2 cycles/100 ka were formed during both the rise and the fall (Fig. 3, A and B). However, where a low subsidence rate is used (0.025 m/ka), although 2 cycles /100 ka are formed on the rise, only 1 cycle/100 ka is commonly formed during the fall (Fig. 3, C and D). This tends to increase the length of the average cycle period, which in turn increases the amount of subsidence per period, so that the apparent amplitude of the long-term sea-level fluctuation is depressed (Fig. 1B). In the extreme case where no cycles are formed during the fall, the apparent sea-level curve defined by the Fischer plot would be horizontal. The modeling predicts that maximum amplitudes will be defined by the Fischer plots where subsidence rates allow the same number of cycles to form on the rise as on the fall. In areas of lower subsidence rate, where fewer cycles are formed during the fall compared to the rise, the plots will underestimate the amplitude of the relative sea-level fluctuation. Note also that omission of cycles during the fall results in the Fischer plots underestimating the rate of sea-level rise (because cycles formed during the rise are assigned an overestimated average period). In a similar manner, they may overestimate the rate of sea-level fall. The Fischer plots become increasingly skewed toward the right as more cycles are omitted during the fall.

RELATIVE SEA-LEVEL CURVES AND FISCHER PLOTS, EARLY ORDOVICIAN, U.S. APPALACHIANS

Facies Sequences

The Lower Ordovician sequence is 0 to 1200 m thick; it thickens into depocenters and thins over arches and onto the craton (Read, 1988a,

1988b). It consists of several stacked third-order sequences of 2 to 5 m.y. duration that are commonly tens of metres to 200 m thick. The sequences show a zoned distribution across depositional strike (Nguyen et al., 1985; Hardie and Shinn, 1986; Bova and Read, 1987). The western platform interior facies are dominated by shallowing-upward peritidal sequences. The carbonate cycles have sharp bases overlain by ooid-skeletal-intraclast grainstone and thrombolitic bioherms (subtidal), grading up into ripple cross-laminated, peloidal ribbon carbonates (restricted subtidal to lower intertidal), and are capped by mud-cracked cryptalgal laminites (intertidal to supratidal facies). Each cycle depicts progradation of muddy tidal flats basinward over shallow subtidal facies. Some laminite caps are intercalated with thin beds of quartz arenite, or contain admixed quartz sand. Other cycles are capped by breccias that result from prolonged subaerial exposure (caliches) and/or evaporite-solution collapse. Toward the outer shelf in Virginia, some intervals lack tidal-flat caps, but still consist of upward-shallowing cycles of deeper subtidal, storm-deposited limestones, locally overlain by subtidal, ripple cross-laminated peloidal grainstone and capped by subtidal algal bioherms with scalloped erosional tops (tidal rock platforms or microkarst) that are locally veneered with lime sand (Bova and Read, 1987).

Relative Sea-Level Curves

The chronostratigraphic diagram and sea-level curve in Figure 4 (Read, 1988b) was constructed from information in Bova and Read (1987), Donaldson (1959), Fisher (1977), Hobson (1963), Lees (1967), Ross et al. (1952), Sando (1957), Spelman (1966), Nguyen et al. (1985), and Hardie and Shinn (1986), who also presented a relative sea-level curve for the lower part of the sequence. The relative sea-level curve (Fig. 4) was constructed by using relative water depths of lithofacies; storm-deposited subtidal muddy carbonates, subtidal algal bioherms, peritidal cyclic limestones, cyclic dolomites, and quartz sands were used as deep- to shallow-water indicators. Relatively open-marine facies are inferred to form during long-term rises because of increased accommodation space favoring slightly deeper, open-marine conditions, whereas more restricted facies develop during a long-term fall due to decreased accommodation space. The relative sea-level curve (Fig. 4) was constructed independently of the Fischer plots (Fig. 5). The large-scale transgressive-regressive events in Figure 4 are traceable throughout much of the Appalachians; they span two depocenters and the intervening Virginia arch and subsidence rates from less than 0.01 m/ka to over 0.04 m/ka (inset map, Fig. 5; Read, 1988a, 1988b). Thus, we do not think that they represent pulses of subsidence, but instead reflect eustatic, third-order sea-level fluctuations.

Fischer Plots, Ordovician Appalachians

The Fischer plots (Fig. 5) include a section from Nittany arch, Pennsylvania (R. K. Goldhammer, unpub. data) and three sections from Virginia (J. F. Read, unpub. data; Bova and Read, 1987) that span 500 km. The Pennsylvanian plot spans the Nittany Dolomite and lower Axeman Limestone; the Virginia plots span the Chepultepec and Kingsport-Mascot Formations. Only the Goodwins Ferry section spans the total Upper Knox sequence. The base of the Ordovician is difficult to define; for mapping purposes it is taken to be above the last thick sands of the Lower Knox Group. The DNAG time scale (Palmer, 1983) was used to construct the plots, 20 Ma being assigned to the Early Ordovician. Because of the limited radiometric control on the geologic column, subsidence rates are calculated from stratigraphic thicknesses for which age constraints are available (base of Early Ordovician to base of Middle Ordovician). If the same time scale is used for all plots, the actual time value used will not affect the magnitude of the sea-level departure, but only the steepness of the curve. This is because this time value is used in calculation of subsidence (thickness/time) and average cycle period (time/number of cycles). As a consequence, using too long or too short a time duration will only expand or contract the curve along the time axis. Average cycle period is calculated by (duration of formation [m.y.] × thickness of measured cyclic section) divided by (number of cycles in the measured section × thickness of formation). For the plots, covered intervals are subdivided into cycles based on calculated average cycle thickness, so that they plot as a horizontal line. Covered intervals in the Ordovician sections used were only 0% to 7% of the total stratigraphic thickness. The Early Ordovician sequences typically lack significant shale and consist of dolomite or limestone throughout, suggesting that they underwent relatively uniform compaction; however, if parts of sections did contain thick shales, this would have to be taken into account in estimating average cycle period and subsidence rate.

The sequences span part or all of relative sea-level cycles O-2 to O-6, and the Fischer plots consistently define these events at all localities (cf. Figs. 4 and 5). The Fischer plots (Fig. 5) include sequences whose cycles are all capped by laminites (e.g., Pennsylvania section), as well as parts of sequences dominated by upward-shallowing subtidal cycles (Avens Bridge). Thus, the plots work equally well in laminite-capped sequences and subtidal sequences that shallow to sea level.

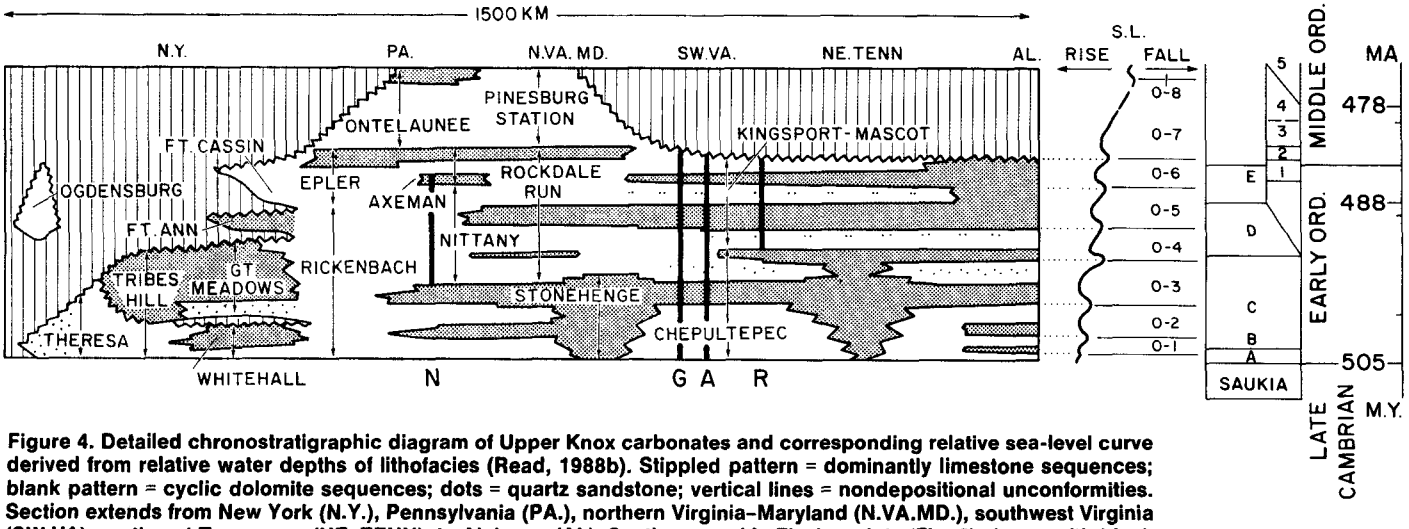

Figure 4. Detailed chronostratigraphic diagram of Upper Knox carbonates and corresponding relative sea-level curve derived from relative water depths of lithofacies (Read, 1988b). Stippled pattern = dominantly limestone sequences; blank pattern = cyclic dolomite sequences; dots = quartz sandstone; vertical lines = nondepositional unconformities. Section extends from New York (N.Y.), Pennsylvania (PA.), northern Virginia–Maryland (N.VA.MD.), southwest Virginia (SW.VA), northeast Tennessee (NE. TENN), to Alabama (AL). Sections used in Fischer plots (Fig. 6) shown with black bars labeled N (Nittany arch), G (Goodwins Ferry), A (Avens Bridge), and R (Rose Hill).

The Fischer plots define third-order depositional sequences of Vail et al. (1984). For these plots, it is assumed that mean subsidence is linear, such that deviations from the horizontal datum reflect either eustatic sea-level changes or changes in subsidence rate. The fact that the Fischer plots are similar, net deviation maxima (highs) and minima (lows) plotting at approximately the same times, supports a eustatic interpretation.

The long-term, third-order deviations stem from the cumulative effect of progressive changes in thicknesses of small-scale carbonate cycles plotted against a mean value. These systematic vertical variations in the stacking patterns of individual cycles define the depositional systems tracts (Vail, 1987) within the third-order sequences. The cycles that plot on the rising part of the third-order deviation (peaking at maximum positive departure) compose the transgressive systems tract. These carbonate cycles have relatively open marine facies, contain the least early dolomite, and, on the outer shelf, commonly lack tidal-flat caps (Nguyen et al., 1985; Bova and Read, 1987). Cycles may progressively thicken upward in response to increasing third-order accommodation potential generated by rising sea level. The deviation maximum (maximum positive departure within a third-order sequence) equates to the maximum flooding surface (Vail, 1987) or condensed interval (Vail et al., 1984), approximating the net eustatic highstand of sea level. Cycles that plot on the falling limb of the third-order deviation (culminating in a sequence boundary) constitute the highstand systems tract, characterized by

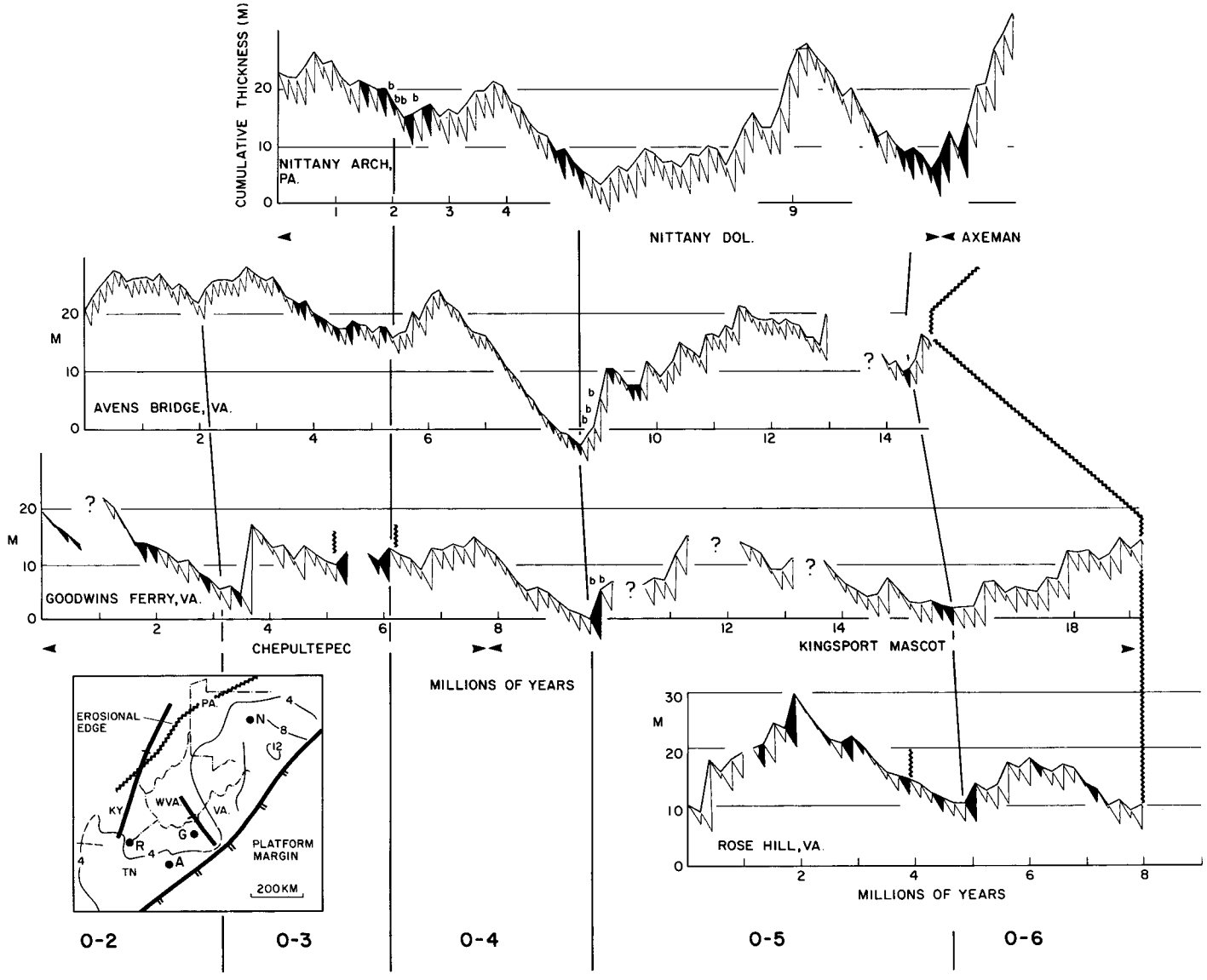

Figure 5. Fischer plots of Early Ordovician Upper Knox–Beekmantown carbonates, from Nittany arch, Pennsylvania, and Avens Bridge, Goodwins Ferry, and Rose Hill areas of Virginia; inset map on palinspastic base shows location of measured sections and isopachs (in hundreds of metres) of Early Ordovician sequence. N = Nittany arch (subsidence rate 0.029 m/ka, cycle period 158 333 yr); A = Avens Bridge (subsidence rate 0.023 m/ka, cycle period 119 760 yr); G = Goodwins Ferry (subsidence rate 0.186 m/ka, cycle period 186 915); R = Rose Hill (subsidence rate 0.0175 m/ka, cycle period 195 142 yr). On Fischer plots, third-order rises in sea level are indicated by rise in curve toward right; third-order falls shown by fall in curve toward right. Black = quartz sand–bearing cycles; b = breccias. Plots define third-order sea-level curves (labeled O-2 to O-6 in Figure 4) consistently at each locality. Quartz sands tend to be associated with falls and lowstands, except in inner platform areas (Rose Hill), where they may occur scattered throughout section. Thick, subtidal-dominated cycles that may lack laminite caps (Bova and Read, 1987) occur on third-order rises O-2, O-3, and O-4. Thus, plots work equally well in subtidal, upward-shallowing cycles that shallow to sea level (Avens Bridge), as in sequences composed totally of laminite-capped cycles (Nittany). Lowest point on plot (lowstand of O-4 cycle) contains regional breccia horizons that correlate with major unconformity in New York State.

carbonate cycles that progressively thin upward in the sequence, are relatively restricted, and contain the most early dolomite. They reflect decreasing third-order accommodation potential resulting from eustatic fall superimposed on subsidence. Carbonate cycles capped with quartz sand straddle the sequence boundaries, thus indicating siliciclastic influx from the cratonic hinterland; this suggests a siliciclastic bypass response associated with lowstand conditions at or near sequence boundaries.

In areas of low subsidence rate (Goodwins Ferry), amplitudes of the plots are lower than those with high subsidence rates (Avens Bridge; Fig. 5). The area with the lower subsidence rate probably has many cycles omitted on the fall compared with the area with the higher subsidence, and thus has lower amplitudes, as predicted by the modeling.

Nonrecognition of one or two cycle boundaries has little effect on the large-scale curves defined by the Fischer plots, but it does affect the smaller scale departures. The plots show a high-frequency signal between 200 ka and 1 Ma; these may prove to be 400 and 800 ka Milankovitch signals.

A crude test of whether the curves are documenting sea-level changes can be done by replotting the data using thermal subsidence rate and cycle thicknesses corrected for sediment-load–induced subsidence. This is documented in Bond et al. (in prep.), who also incorporate corrections for compaction. If S is subsidence due to sediment loading, ρm and ρs are mantle and water-saturated sediment densities (3.3 and 2.3 g/cm^3, respectively), ΔTS is space created by thermal subsidence and/or sea-level rise or fall, and Z is total sediment thickness due to thermal subsidence, sea-level rise or fall, and sediment loading, then

$$S\frac{(\rho m - \rho s)}{\rho s} = \Delta TS,$$

$$S = 2.3\ \Delta TS,$$

and

$$Z = 3.3\ \Delta TS, \text{ or } \Delta TS = 0.3\ Z.$$

If there is no sea-level rise, then backstripping the sediment load should give the amount of thermal subsidence, which is roughly linear in the short term and has a rate of 0.3 times total stratigraphic thickness/time duration of formation. After backstripping each cycle, any departure from the thermal subsidence curve must represent the amount of sea-level fluctuation. Thus, the change in sea level (ΔSL) at any time is

ΔSL = 0.3 cumulative cycle thickness – (thermal subsidence rate × time).

Rerunning the Fischer plots using this last equation has the effect only of reducing the amplitudes of the plots by one-third. Thus, the Fischer plots in Figure 5 can be read as eustatic sea-level records if the vertical scale is decreased in magnitude to one-third (i.e., for 10 m read 3 m). This suggests that the recorded eustatic signals range from 2 to 10 m. These are probably minimum amplitudes, because the highstand peaks on the plots probably occur later than they do in reality, due to actual cycle periods during the rise likely being shorter than cycle periods during the fall. Moving the peaks to the left to correct for this would have the effect of increasing the amplitude of the sea-level fluctuations.

Correlation Using Fischer Plots

The Fischer plots also provide a valuable correlation tool that could prove useful in cyclic sequences of widely differing thicknesses in which biostratigraphic control is typically poor. As the Fischer plots are graphed against time, the positions of third-order highstands, lowstands, and quartz sandy cycles provide a means of correlating between sections.

CONCLUSIONS

Fischer plots in which cumulative cycle thickness corrected for linear subsidence is plotted against time (using an average cycle period) provide an objective method of recognizing third-order sea-level fluctuations in peritidal cyclic carbonates.

REFERENCES CITED

Bova, J.A., and Read, J.F., 1987, Incipiently drowned facies within a cyclic peritidal continental ramp sequence, Chepultepec interval, Virginia Appalachians: Geological Society of America Bulletin, v. 98, p. 714–727.

Donaldson, A.L., 1959, Stratigraphy of the Lower Ordovician Stonehenge and Larke formations in central Pennsylvania [Ph.D. thesis]: State College, Pennsylvania, Pennsylvania State University, 393 p.

Fischer, A.G., 1964, The Lofer cyclothems of the Alpine Triassic: Geological Survey of Kansas Bulletin, v. 169, p. 107–149.

Fisher, D.W., 1977, Correlation of the Hadrynian, Cambrian and Ordovician rocks in New York State: New York State Museum Map and Chart Series No. 25, 75 p.

Goldhammer, R.K., 1987, Platform carbonate cycles, Middle Triassic of northern Italy: The interplay of local tectonics and global eustasy: [Ph.D. thesis]: Baltimore, Maryland, Johns Hopkins University, 468 p.

Goldhammer, R.K., Dunn, P.A., and Hardie, L.A., 1987, High frequency glacio-eustatic sea level oscillations with Milankovitch characteristics recorded in the Middle Triassic platform carbonates in northern Italy: American Journal of Science, v. 287, p. 853–892.

Hardie, L.A., and Shinn, E.A., 1986, Carbonate depositional environments, modern and ancient; 3, Tidal flats: Colorado School of Mines Quarterly, v. 81, 74 p.

Hobson, J.P., 1963, Stratigraphy of the Beekmantown Group in southeastern Pennsylvania: Pennsylvania Geological Survey Bulletin G 37, 331 p.

Lees, J.A., 1967, Stratigraphy of the Lower Ordovician Axeman Limestone of central Pennsylvania: Pennsylvania Geological Survey Bulletin G 52, 78 p.

Nguyen, C., Goldhammer, R.K., and Hardie, L.A., 1985, Depositional facies mosaics and their time lines in the Lower Ordovician carbonates of the central Appalachians [abs.]: American Association of Petroleum Geologists Bulletin, v. 69, p. 292.

Palmer, A.R., 1983, The Decade of North American Geology 1983 geologic time scale: Geology, v. 11, p. 503–504.

Read, J.F., 1988, Evolution of Cambro-Ordovician passive margin, U.S. Appalachians, *in* Hatcher, R.D., Jr., et al., eds., The Appalachian-Ouachita orogen in the United States: Boulder, Colorado, Geological Society of America, The Geology of North America, v. F-2 (in press).

——1988b, Controls on evolution of Cambrian-Ordovician passive margin, U.S. Appalachians, *in* Crevello, P., et al., eds., Controls on carbonate platform and basin development: Society of Economic Paleontologists and Mineralogists Special Publication 44 (in press).

Read, J.F., Grotzinger, J.P., Bova, J.A., and Koerschner, W.F., 1986, Models for generation of carbonate cycles: Geology, v. 14, p. 107–110.

Ross, R.J., et al., 1952, The Ordovician System in the United States: International Union of Geological Sciences Publication no. 12, 73 p.

Sando, W.J., 1957, Beekmantown Group (Lower Ordovician) of Maryland: Geological Society of America Memoir 68, 161 p.

Spelman, A. R., 1966, Stratigraphy of the Lower Ordovician Nittany Dolomite in central Pennsylvania: Pennsylvania Geological Survey, 4th Series, Bulletin G 47, 187 p.

Vail, P.R., 1987, Seismic stratigraphy interpretation procedure, *in* Bally, A.W., ed., Seismic stratigraphy folio series: Tulsa, Oklahoma, American Association of Petroleum Geologists, p. 1–11.

Vail, P.R., Mitchum, R.M., Jr., and Thompson, S., III, 1977, Seismic stratigraphy and global changes of sea level, Part 4: Global cycles and relative changes of sea level, *in* Payton, C.E., ed., Seismic stratigraphy; applications to hydrocarbon exploration: American Association of Petroleum Geologists Memoir 26, p. 83–97.

Vail, P.R., Hardenbol, J., and Todd, R.G., 1984, Jurassic unconformities, chronostratigraphy, and sea-level changes from seismic stratigraphy and biostratigraphy, *in* Schlee, J., ed., Interregional unconformities and hydrocarbon accumulation: American Association of Petroleum Geologists Memoir 36, p. 129–144.

ACKNOWLEDGMENTS

Partly supported by National Science Foundation Grants EAR 8108577 and EAR 8305878, and by grants from Texaco and Chevron oil companies to J. F. Read. L. A. Hardie suggested trying Fischer plots on the Cambrian-Ordovician sequence in Virginia. We thank G. C. Bond and L. A. Hardie for their critical reviews, and D. Osleger, M. Elrick, I. Montanez, and R. Barnaby. Sriram S. did the computer programming and T. Agliata did the drafting.

Manuscript received November 6, 1987
Revised manuscript received June 7, 1988
Manuscript accepted June 21, 1988